



Contents lists available at ScienceDirect

Engineering Science and Technology, an International Journal

journal homepage: www.elsevier.com/locate/jestch

Multibeam-based mmWave segmented beamforming array system for high efficiency and secure communication

Seung-Won Oh, Woo-Hee Lim, Han Lim Lee *

School of Electrical and Electronics Engineering, Chung-Ang University, Seoul 06974, South Korea

ARTICLE INFO

Keywords:

High-efficiency Tx
mmWave beamforming communication
Multibeam array antenna
Phased array antenna
Secure data transmission
Segmented beamforming array

ABSTRACT

A new mmWave transmitter architecture with multibeam-based segmented beamforming arrays (SBAs) for high-efficiency and secure communication is proposed. Unlike conventional communication architecture, which transmits a high-order QAM signal through a single RF-chain, the proposed structure transmits independently controlled multiple QPSK signals to form M-QAM signals. The multiple independent SBA chains radiate independent QPSK signals at each chain's maximum operation efficiency to reduce the peak-to-average-power ratio. Then, multiple beams with QPSK signals are steered by the SBAs to form a line of combination (LoC) where multiple QPSK signals are spatially vector-combined to generate M-QAM signals correctly. For any unidentified receiver outside the LoC, the desired high-order QAM signals cannot be retrieved owing to the lack of required sets of QPSK signals and SBA steering information. Thus, higher data security can be also guaranteed. To verify the proposed architecture, 28-GHz SBA-based transmitter and reference receiver were implemented. Three QPSK signal sets were transmitted by three SBAs supporting independent beamforming to flexibly create a narrow LoC where the receiver retrieved 64-QAM signals successfully. Furthermore, secured data transmission was verified with an extra eavesdropper in the vicinity of the target receiver. By controlling the LoC, only the target receiver successfully demodulated the 64-QAM signals.

1. Introduction

As 5G networks have been practically and widely established all around the world, the demand for realizing efficient mmWave communication is rapidly increasing [1–3]. With the evolution of communication generations, the required measure of system performance has risen to meet potential advanced standards while considering practical adoptability for commercialization. To maximize the achievable data rate in mmWave communications, high-order quadrature amplitude modulation (QAM) must also be effectively accompanied by mmWave transceivers [4,5]. However, the overall system performance degradation unavoidably occurs in mmWave owing to high propagation loss, low power consumption efficiency, and unwanted coupling in mmWave circuits [6–8]. Because the power amplifier (PA) consumes the highest power in a typical communication architecture, a large number of low-efficiency PAs in a large-scale array antenna critically reduces the overall system efficiency. Moreover, the system efficiency for high-order QAM signal transmission degrades even more rapidly because of a sharp decrease in PA efficiency below its 1-dB compression point (P1-dB) [9].

In particular, as the peak-to-average-power ratio (PAPR) increases for orthogonal frequency division multiplexing with high-order QAM, the difficulty in designing a high-efficiency transmitter (Tx) due to low PA back-off efficiency must be resolved systematically [10]. Although PAPR can be reduced by using a digital predistortion (DPD) technique [11], DPD-based approaches increase both circuit and control complexity. In addition, crosstalk in the Tx should be more carefully managed. Another approach employing the spectral mask filling method that utilizes unused subcarriers in a guard band can be used to reduce PAPR [12]. However, this method is unsuitable for stable data communication owing to the limited sensitivity of PA frequency response. Because next-generation system architectures such as massive multiple-input multiple-output (MIMO) and phased array require a very large number of RF chains compared to conventional systems, PAPR and power consumption are considered the key toward the successful adoption of mmWave technology. Specifically, an effective method that minimizes RF power consumption of the entire system and maximizes system efficiency by considering both transceiver and antenna configurations needs to be investigated [13–16].

* Corresponding author.

E-mail address: hanlimlee@cau.ac.kr (H.L. Lee).<https://doi.org/10.1016/j.jestch.2024.101676>

Received 10 November 2023; Received in revised form 15 February 2024; Accepted 15 March 2024

Available online 23 March 2024

2215-0986/© 2023 Karabuk University. Publishing services by Elsevier B.V. This is an open access article under the CC BY-NC-ND license (<http://creativecommons.org/licenses/by-nc-nd/4.0/>).

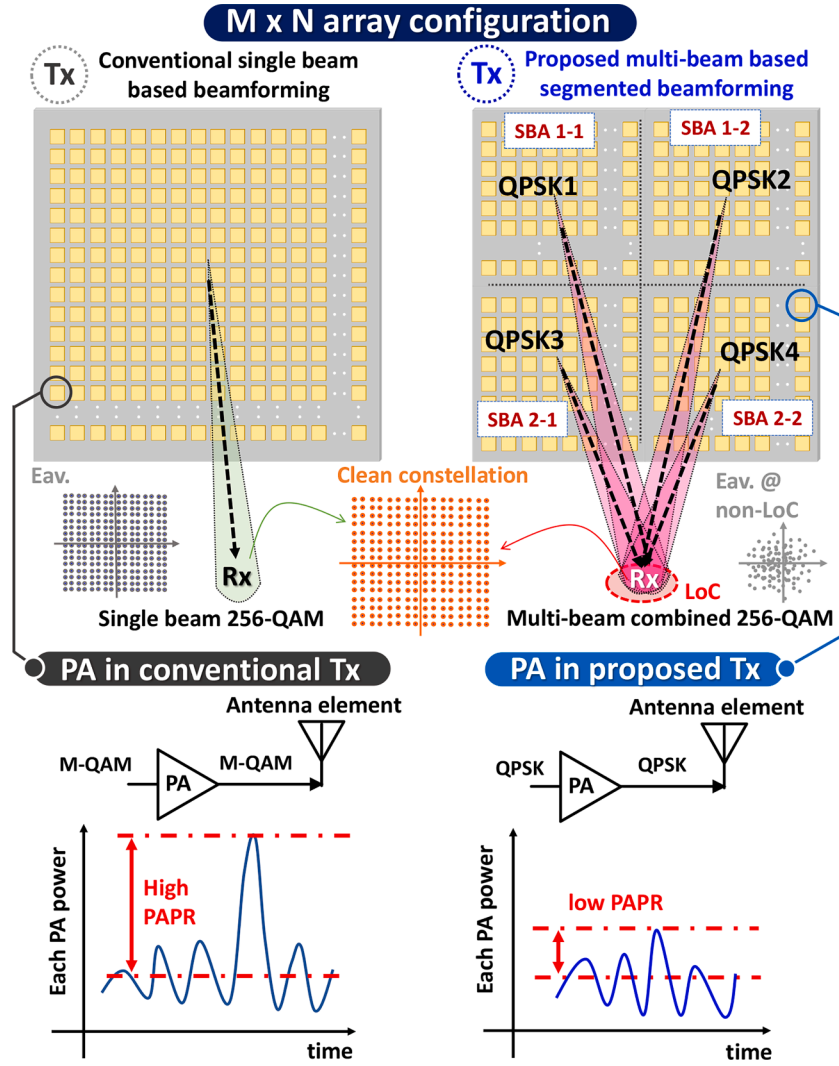


Fig. 1. Segmented beamforming array-based Tx for high-order QAM generation with reduced PAPR and enhanced security communication.

In this paper, a new communication system based on a multibeam spatial vector-combining architecture with a segmented beamforming technique is proposed. The proposed architecture uses multiple segmented beamforming arrays (SBAs) for transmitting multiple independent QPSK modulated signals instead of high-order M-QAM signals directly through a single chain as described in Fig. 1. The multiple beams with QPSK signals are steered by the SBAs to form a line of combination (LoC) where multiple beams are spatially vector-combined to correctly generate high-order QAM signals. Because each QPSK signal has less nonlinear distortion than high-order QAM and can be transmitted at a higher PA efficiency owing to reduced back-off operation, the problems in the conventional Tx architecture can be alleviated. Given the fact that QPSK has lower PAPR compared to high order M-QAM [17–19], the unavoidable high-PAPR problem can be effectively solved by lowering both modulator and PA performance burdens. The circuit loss and complexity can be efficiently improved by generating high-order QAM signals from only QPSK or low-order QAM signals. Furthermore, point-to-point communication through LoC formation with multiple beams enables the implementation of a system with improved security. Because eavesdroppers outside the LoC lack the required complete QPSK sets and the SBA steering sequences are unknown, they cannot retrieve the desired signals correctly.

Therefore, higher communication security can be guaranteed by using the proposed multibeam-based SBA communication system.

2. Design and analysis of the proposed mmWave SBA transmitter

2.1. Analysis of the proposed SBA-based architecture

In this section, the structural configuration of the proposed multibeam-based SBA Tx and its exemplar 64-QAM generation are described. The proposed SBA Tx is aimed at forming a high-order QAM using several QPSK signals while always maintaining PA operation near its peak efficiency to avoid back-off efficiency degradation as displayed in Fig. 2 (a). The output of each SBA is optimized to have relatively half the power from one to the other. In a general high-order QAM transmission, one serial data stream source is fed to the higher-order modulation stage block. The serial data stream is separated into odd and even bits through a serial-to-parallel converter, and the separated bit stream generates multilevel data signals $I(t)$ and $Q(t)$ through a level converter. $I(t)$ and $Q(t)$ are modulated and added through sinusoidal and cosine waves, respectively, with carrier frequency f_c and transmitted. The general modulated QAM signal can be expressed as (1):

$$S_{QAM} = A(I(t)\cos 2\pi f_c t - Q(t)\sin 2\pi f_c t) \quad (1)$$

where A denotes the amplitude of the carrier signal.

By contrast, the proposed SBA Tx architecture is configured with a parallel data stream distribution sequence for multiple individual QPSK

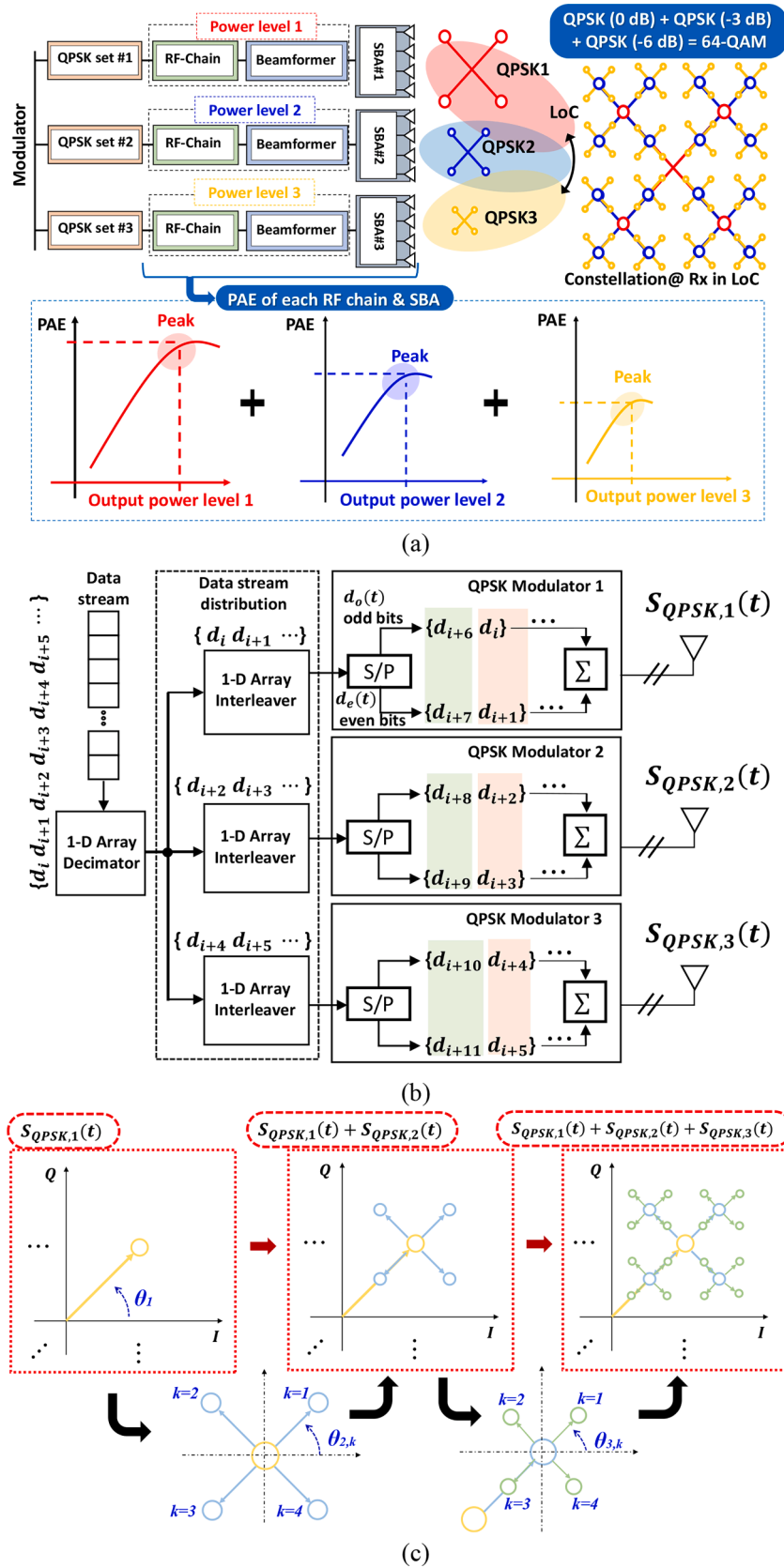


Fig. 2. Proposed multibeam-based SBA with (a) PAs operating near the peak power-added efficiency, (b) individually distributed modulator blocks, and (c) spatially vector-summed QPSKs for high-order QAM generation.

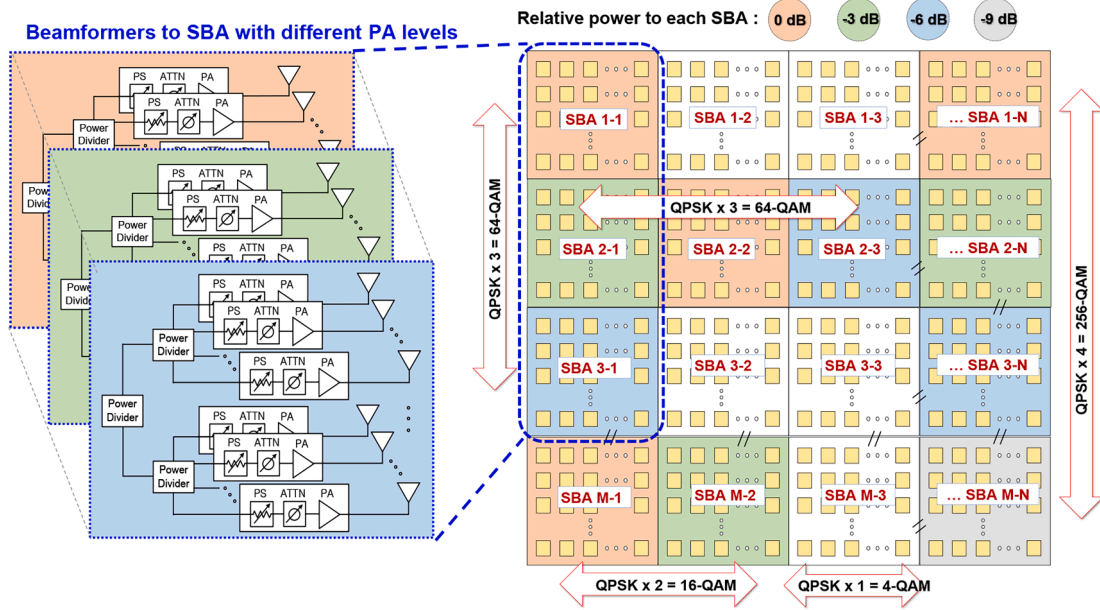


Fig. 3. Proposed SBA with two-dimensional extension for massive-MIMO beamforming.

modulation stages as displayed in Fig. 2 (b). Although a single data stream source is used as in the conventional QAM modulation scheme, three individual QPSK modulators are used to form 64-QAM signals. Specifically, the 64-QAM data stream is divided into three parallel data sets with even unit bits by a one-dimensional array decimator. Then, each data set is fed to the QPSK modulators individually instead of a single 64-QAM modulator. For example, the data stream is divided into two-bit units and distributed to three QPSK modulators with the serial input data stream denoted by d_i ($i = \text{integer}$) as follows:

$$QPSK|_i = [d_i, d_{i+1}, d_{i+6}, d_{i+7}, \dots] \quad (2)$$

$$QPSK|_{i+1} = [d_{i+2}, d_{i+3}, d_{i+8}, d_{i+9}, \dots] \quad (3)$$

$$QPSK|_{i+2} = [d_{i+4}, d_{i+5}, d_{i+10}, d_{i+11}, \dots] \quad (4)$$

Then, these subdivided data sets are modulated through a serial-to-parallel converter to generate data symbols $S_{QPSK,i}$. The general QPSK message symbol can be expressed as (5), where E_s and T_s denote the symbol energy and symbol duration, respectively.

$$\begin{aligned} S_{QPSK}(t) &= \sqrt{\frac{2E_s}{T_s}} \cos\left(2\pi f_c t + \frac{2\pi m}{4}\right) \quad (m = 0, 1, 2, 3) \\ &= \sqrt{E_s} \cdot \cos\left(\frac{2\pi m}{4}\right) \cdot \sqrt{\frac{2}{T_s}} \cdot \cos(2\pi f_c t) \\ &\quad - \sqrt{E_s} \cdot \sin\left(\frac{2\pi m}{4}\right) \cdot \sqrt{\frac{2}{T_s}} \cdot \sin(2\pi f_c t). \end{aligned} \quad (5)$$

As described before, sequential $S_{QPSK,i}$ in the proposed configuration must have half the amplitude relative to a former QPSK set fed to its neighboring Tx chain. Thus, unlike the conventional S_{QPSK} expression in (5), the proposed $S_{QPSK,i}$ ($i = 1, 2, 3$) are expressed as

$$\begin{aligned} S_{QPSK,1}(t) &= \sqrt{E_s} \cdot d_{1,I}(t) \cdot \sqrt{\frac{2}{T_s}} \cdot \cos(2\pi f_c t) - \sqrt{E_s} \cdot d_{1,Q}(t) \cdot \sqrt{\frac{2}{T_s}} \\ &\quad \cdot \sin(2\pi f_c t) \end{aligned} \quad (6)$$

$$\begin{aligned} S_{QPSK,2}(t) &= \frac{1}{2} \sqrt{E_s} \cdot d_{2,I}(t) \cdot \sqrt{\frac{2}{T_s}} \cdot \cos(2\pi f_c t) - \frac{1}{2} \sqrt{E_s} \cdot d_{2,Q}(t) \cdot \sqrt{\frac{2}{T_s}} \\ &\quad \cdot \sin(2\pi f_c t) \end{aligned} \quad (7)$$

$$\begin{aligned} S_{QPSK,3}(t) &= \frac{1}{4} \sqrt{E_s} \cdot d_{3,I}(t) \cdot \sqrt{\frac{2}{T_s}} \cdot \cos(2\pi f_c t) - \frac{1}{4} \sqrt{E_s} \cdot d_{3,Q}(t) \cdot \sqrt{\frac{2}{T_s}} \\ &\quad \cdot \sin(2\pi f_c t) \end{aligned} \quad (8)$$

Because the terms $\sqrt{\frac{2}{T_s}} \cos(2\pi f_c t)$ and $-\sqrt{\frac{2}{T_s}} \sin(2\pi f_c t)$ form a signal space in a typical orthogonal basis, the message symbol can be expressed in a vector form composed of in-phase and quadrature-phase components. Thus, the data symbols $S_{QPSK,i}$ from Fig. 2 (b) can be expressed in polar form as follows,

$$S_{QPSK,i}(t) = \alpha \cdot e^{j\theta_{i,k}} \quad (9)$$

$$S_{QPSK,i+1}(t) = \left(\frac{\alpha}{2}\right) \cdot e^{j\theta_{i+1,k}} \quad (10)$$

$$S_{QPSK,i+2}(t) = \left(\frac{\alpha}{4}\right) \cdot e^{j\theta_{i+2,k}} \quad (11)$$

where α and $\theta_{i,k}$ ($i = 1, 2, 3$ and $k = 1, 2, 3, 4$) denote the amplitude and phase, respectively, for each QPSK symbol. These QPSK symbol sets are individually fed to mmWave up-converters and beamforming array antennas. Because each Tx chain only drives QPSK signals, more power-efficient transmission can be facilitated compared to the single-chain direct 64-QAM signal transmission. Then, each QPSK beamforming array radiates the electromagnetic signals. If all three beams are combined at a target region following (9)-(11), the LoC where spatial vector summation can be conducted for a receiver (Rx) to correctly retrieve 64-QAM signals can be created. Within the LoC region, multibeam vector summation can be obtained as depicted in Fig. 2(c) according to (12):

$$C_A = S_{QPSK,1}(t) + S_{QPSK,2}(t) + S_{QPSK,3}(t) \quad (12)$$

Furthermore, unlike the conventional data transmission, higher data security can be achieved because eavesdroppers cannot be fully located within the narrow LoC region, receiving scrambled data that cannot be combined according to (9). Because 64-QAM signals are segmented into multiple QPSK sets and combined through multibeam beamforming operation when being transmitted, each beamforming array chain corresponds to SBA in the proposed architecture. Similarly, other alternative data transmissions such as 16-QAM using two QPSK sets, 64-QAM using one QPSK and one 16-QAM set each, or 256-QAM using four QPSK sets can also be formed through the proposed SBA architecture. Thus,

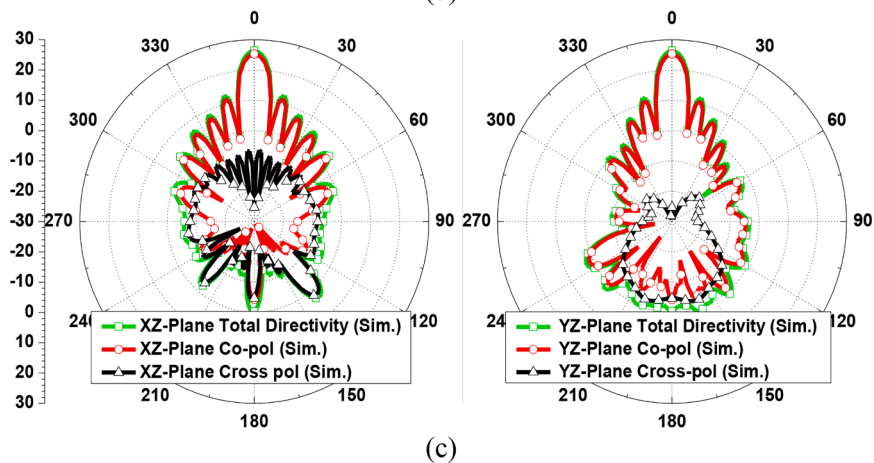
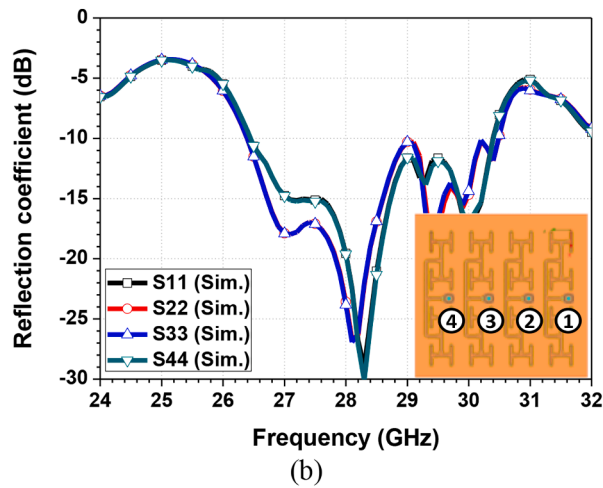
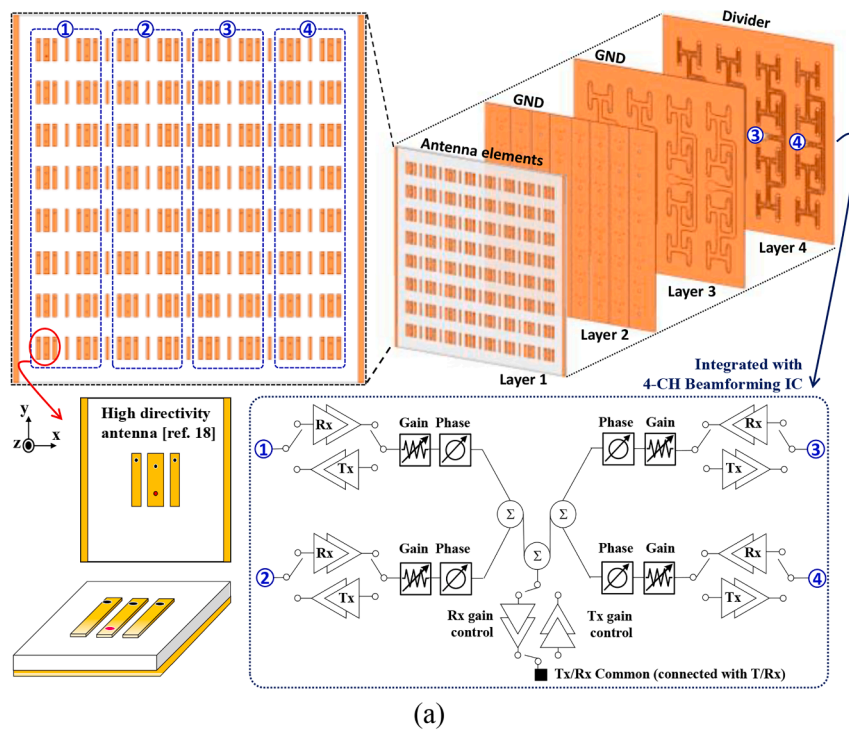


Fig. 4. SBA configuration with (a) high-directivity antenna [20] array and 4-ch beamforming IC, (b) simulated reflection coefficients, and (c) simulated radiation patterns of 8×8 array in xz and yz planes at 28 GHz.

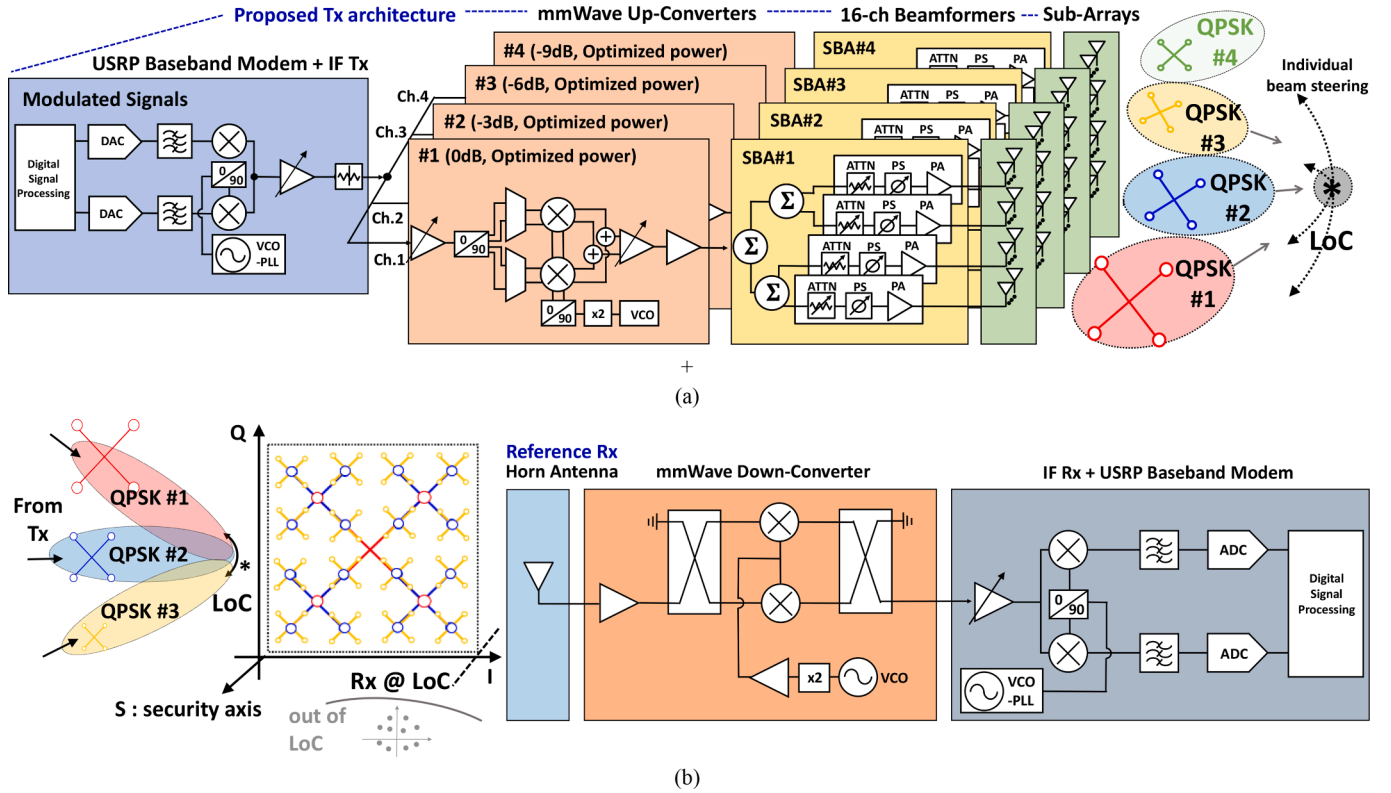


Fig. 5. Overall communication system architecture with the (a) proposed multibeam-based SBA Tx and (a) single-channel reference Rx.

highly efficient two-dimensionally extendable MIMO beamforming communications can be implemented by using the proposed SBA technique as illustrated in Fig. 3. Nevertheless, this work focused on the 64-QAM generation to verify the proposed SBA technique through real experiments.

2.2. High-directivity SBA with 4-ch BFIC design

To ensure highly secured data transmission through SBA, a narrow LoC corresponding to high antenna directivity is required. Although an increase in array size can increase antenna directivity, the required number of beamformers inevitably increases, resulting in more power consumption as well as an increase in physical size. To overcome this problem, high-gain antenna elements can be adopted to increase the array antenna directivity while reducing the required array size. Fig. 4 (a) shows the 28-GHz SBA configured by using 8×8 high-gain antenna elements, where a single element called a planar segmented antenna (PSA) has been previously proposed in [20]. In this work, the PSA was expanded and integrated with a 4×64 feed network to be further integrated with a 4-ch mmWave beamforming IC (BFIC). To save cost in the BFIC, each channel is connected to a 2×16 sub-array as marked with a blue dotted box on the array top-view. The SBA is designed with a 4-layer printed circuit board (PCB), while beamformers are integrated externally in a complete module. The antenna element edge-to-edge spacing is $0.373 \lambda_0$, and the ground plane size is $6.4 \lambda_0 \times 6.4 \lambda_0$ at 28 GHz. Fig. 4 (b) shows the simulated reflection coefficients for each port of the SBA with the integrated feed network. The simulated maximum 10-dB impedance bandwidth is 14.75 % with the center frequency of 28 GHz. In addition, Fig. 4 (c) shows the simulated radiation patterns of the SBA with the integrated feed network in both xz and yz planes at 28 GHz. The simulated peak realized gain and total directivity in the xz plane were 25.2 and 26.4 dBi, respectively. Similarly, the simulated peak realized gain and total directivity in the yz plane were 25.2 and 26.4 dBi, respectively. In addition, the simulated half-power beam width

in the xz and yz planes was 8.3° and 8.2° , respectively.

2.3. Multibeam-based mmWave SBA Tx design

The overall system architecture to verify the proposed multibeam-based SBA communication system is depicted in Fig. 5. In the proposed system, both Tx and Rx baseband stages were configured with a software-defined radio such as NI universal software radio peripheral (NI-USRP), which is a reconfigurable RF device that includes an FPGA and RF front-end. Fig. 5 (a) shows the Tx architecture including the proposed mmWave SBA, where each Tx chain is optimized near its peak power-added efficiency (PAE). Further, the Tx is configured by the baseband, intermediate frequency (IF), and mmWave up-converter stages. In the baseband stage, a USRP digital processor and digital-to-analog converters are included. Modulated signals generated from one data stream source are transmitted from the IF to the mmWave stage through multiple channels for segmented beams. In the mmWave stage, four up-converters, 16-channel beamformers comprising four 4-ch BFICs, and mmWave sub-array antennas are included. To retrieve high-order QAM signals from the segmented QPSK beams, a typical Rx is also designed as shown in Fig. 5(b). In the baseband stage of the Rx, USRP digital processor, and analog-to-digital converter are included. In the mmWave stage, a horn antenna and down-converter are included.

For both Tx and Rx baseband and IF, NI LabView communications software was used. The data stream sequence at the transmitter comprises two parts: USRP hardware setting and QPSK signal generation. First, multiple USRP devices were set up by matching the start time through proper triggering. Next, the sampling rate of the signal, carrier frequency of the signal, port settings for antennas, and gains for each antenna port were set up. In addition to start time initialization of the two USRPs, signal synchronization from them was also required. Accordingly, NI CDA-2990, a clock distribution device that supports system synchronization including USRPs, was also employed. Then, parameters such as sample per symbol and filter for QPSK signal

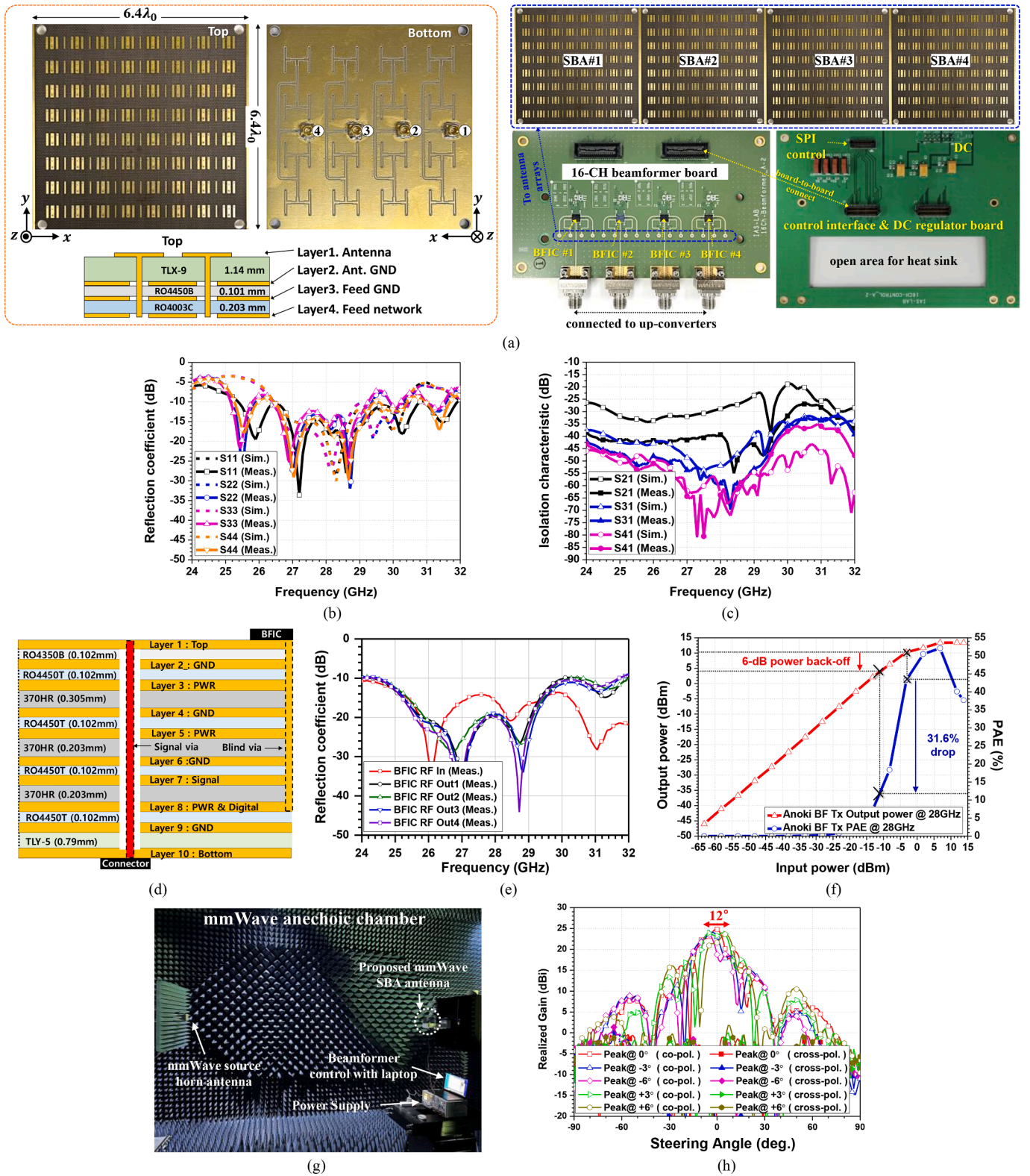


Fig. 6. Proposed SBA module: (a) photo of fabricated SBA module, (b) measured reflection coefficient of array antenna, and (c) isolation of antenna ports; (d) beamformer board layer information, (e) measured reflection coefficient of beamformer RF ports, and (f) beamformer output power with PAE; (g) measurement at mmWave anechoic chamber and (h) measured radiation patterns in the xz plane according to the main beam-steering at 28 GHz.

generation were set. Multiple QPSK signals were generated with the proposed SBA data stream sequence implemented with a bit decimator and bit interleaver. Then, each generated QPSK signal was loaded into two USRPs and transmitted at the IF. These IF signals were individually up-converted to the mmWave SBA chain consisting of up-converters, 4-

ch beamformers, and high-directivity array antennas. To flexibly control the LoC through multiple SBAs, the phases and magnitudes of each SBA were controlled externally through an SPI controller. More details about the implementation of the proposed architecture are given in the next section.

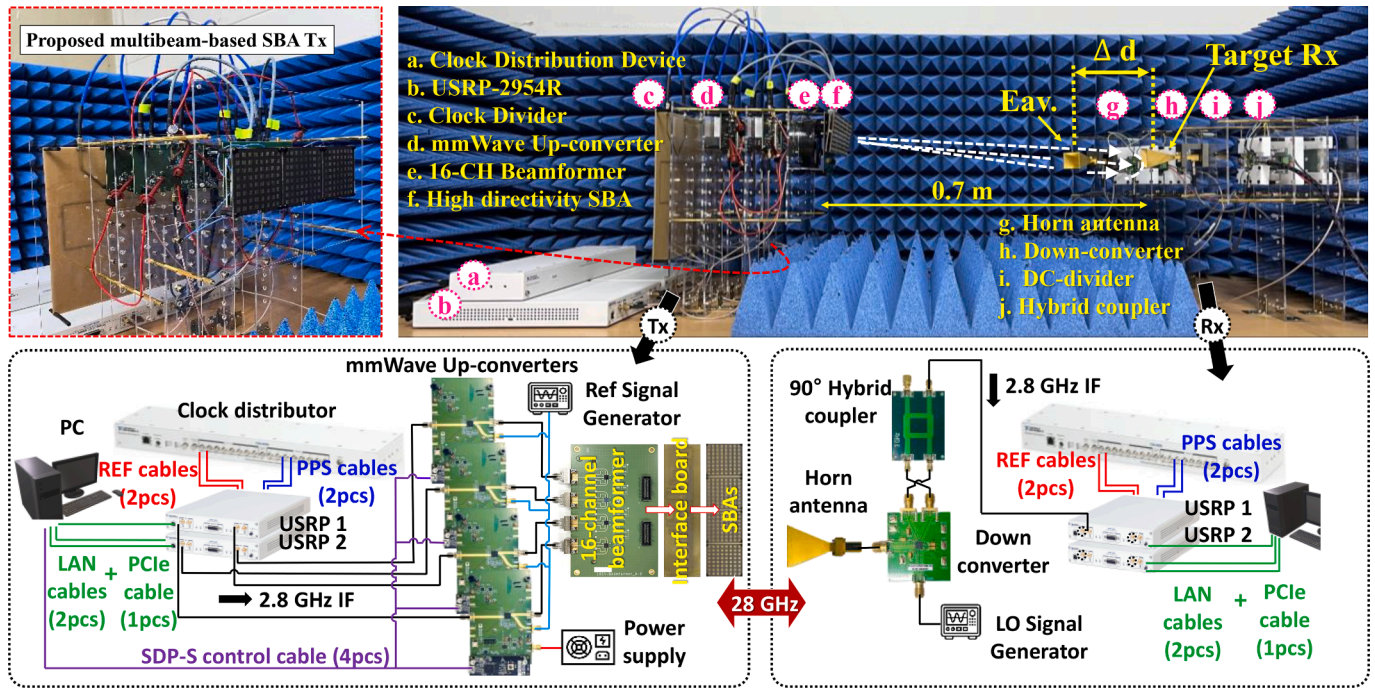


Fig. 7. Implementation of the proposed multibeam-based mmWave SBA Tx and reference Rx, and constellation measurement setup.

3. Fabrication and measurement

3.1. mmWave SBA module fabrication and measurement

First, a single mmWave SBA antenna was fabricated with a four-layer PCB as displayed on the left side in Fig. 6 (a). The Taconic TLX-9 substrate had a relative permittivity of 2.5 and a loss tangent of 0.0019, while the Rogers RO4003C substrate had a relative permittivity of 3.55 and a loss tangent of 0.0027. Furthermore, the Rogers RO4450T was used as a prepreg having a relative permittivity of 3.35 and a loss tangent of 0.004. Fig. 6 (b) and (c) show the simulated and measured reflection coefficient and isolation of the SBA antenna ports, respectively. The measured maximum 10-dB impedance bandwidth of the SBA antenna was 10.7 %, and the minimum isolation was better than 39 dB at 28 GHz. Then, four SBA antennas were fabricated and integrated with the 16-ch beamformer board comprising four 4-ch BFICs as shown at the right side in Fig. 6 (a). The 16-ch beamformer board was fabricated with four AWMF-0162 BFICs from Anokiwave and a 10-layer PCB as displayed in Fig. 6 (d). The Rogers RO4350B substrate had a relative permittivity of 3.66 and a loss tangent of 0.0037, and the Isola 370HR substrate had a relative permittivity of 4.03 and a loss tangent of 0.023. The BFIC supported the n257 band, where the measured reflection coefficient confirmed the 10-dB impedance bandwidth satisfied from 26.5 to 29.5 GHz as shown in Fig. 6 (e). In addition, as the integrated phase shifters and variable-gain amplifiers were 6-bit and 5-bit digitally controlled, the phase and amplitude resolutions within the operation bandwidth were 5.6° and 0.5 dB, respectively. Furthermore, the output power and PAE of the BFIC were measured as shown in Fig. 6 (f). The measured output 1-dB compression point (P1-dB) was approximately 10.3 dBm with a measured PAE of 43.3 %. If the BFIC Tx operated at 6-dB back-off, the PAE decreased to 11.7 %, resulting in a 31.6 % efficiency degradation. For high-order QAM, higher power back-off is required, and thus poorer efficiency is expected. Moreover, as the antenna array scale increases, more PAs are required, causing critical degradation of the total power consumption. By contrast, the proposed SBA transmits QPSK signals near the PA's peak PAE, significantly increasing the total efficiency. Further, Fig. 6 (g) and (h) show the mmWave radiation measurement setup and the measured beam-steering patterns in the xz plane,

respectively. Because the sub-array was grouped in a 2×8 configuration with high-gain antenna elements, the 3-dB steering angle was limited to 12° at 28 GHz.

3.2. Proposed multibeam-based mmWave SBA transmitter and reference receiver implementation

To verify the proposed architecture and SBA-based data transmission, the complete Tx and Rx chains including the USRP-assisted baseband and IF, mmWave up-converters, and mmWave down-converter with a reference horn antenna were implemented as displayed in Fig. 7. For the Tx, the baseband and IF were configured by using the NI USRP-2954R, which supports two Tx and Rx channels each. In this work, two USRPs were used to provide a total of four Tx channels. Further, multiple QPSK signals at the IF 2.8 GHz including the previously described data stream sequence were implemented through the NI LabView communications software. To generate an independently controllable multibeam, two USRP devices were synchronized through the commercially available NI CDA-2990 clock distribution device. The four IF Tx channels of the two USRPs were set to have a relative power difference of 3 dB to verify the proposed multibeam spatial vector combination. Then, four mmWave up-converters were used to translate the modulated QPSK signals from the IF at 2.8–28 GHz. Then, the SBAs discussed in the previous section were connected in the last stage, where each SBA had an independent beam-steering angle of $\pm 6^\circ$. Furthermore, to retrieve the 64-QAM signals transmitted by the SBA-based technique, the reference 28-GHz Rx was also configured by using a mmWave horn antenna and a quadrature signal down-converter. The 28-GHz signals were received at LoC and then down-converted to IF at 2.8 GHz. The IF signals were fed to one Rx channel of the USRP and processed to form the 64-QAM constellation with measured error vector magnitude (EVM).

3.3. 64-QAM performance verification through the proposed multibeam QPSK synthesis and LoC control

As mentioned previously, although four SBA modules were implemented, one was for backup and only three SBAs were used for 64-QAM

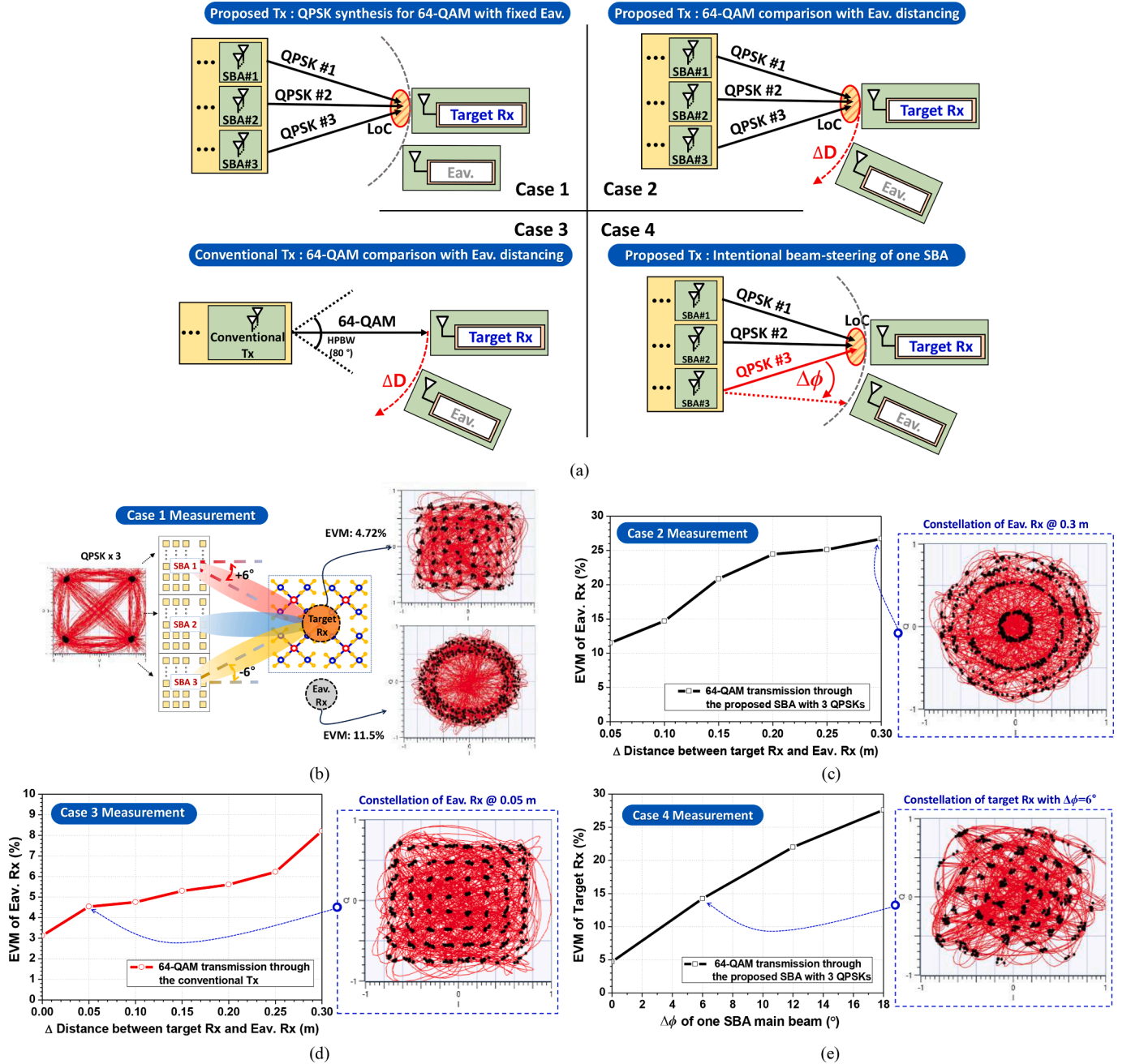


Fig. 8. Different test cases and measured results: (a) measurement configurations and measured results of (b) case 1, (c) case 2, (d) case 3, and (e) case 4.

performance verification. Referring to Fig. 7, an extra Rx was also implemented as an eavesdropper and placed near the target Rx to verify both SBA-based data transmission and secured communications. Thus, four test cases were measured in total as depicted in Fig. 8 (a). First, the 64-QAM signal synthesis and retrieval performance was tested with the proposed SBA-based Tx with the eavesdropper at a fixed distance as displayed in case 1. To form the LoC for the target Rx, two SBA antenna main beams were steered at $\pm 6^\circ$, while the eavesdropper Rx was placed at a distance of 0.05 m from the target Rx as shown in Fig. 8 (b). To achieve a main beam steering angle of 6° , the required phase shift for the antenna elements was approximately 18° . Therefore, the 6-bit phase shifter of the integrated BFIC with a 5.6° phase shift resolution was sufficient for this experiment. Here, the target Rx could retrieve a proper 64-QAM constellation with a measured EVM of 4.72 %, while the eavesdropper Rx was unable to retrieve the transmitted signals with a measured EVM of 11.5 %. Next, the distance between the target Rx and

the eavesdropper Rx was varied as denoted by the test case 2 in Fig. 8 (a). The measured EVM of 27.6 % at $\Delta D = 0.3$ m was observed, proving the successful communication within the LoC and security enhancement outside the LoC. To compare the security performance, the conventional Tx transmitting a single 64-QAM signal was also tested as represented by case 3 in Fig. 8 (a). The measured EVM of the eavesdropper Rx was 4.5 % at $\Delta D = 0.05$ m with a good 64-QAM constellation and still lower than 8.5 % at $\Delta D = 0.05$ m as shown in Fig. 8 (d). At the same ΔD , the measured EVM of the proposed architecture was greater by more than 7 %, proving the improved communication security even with the eavesdropper in the vicinity of the target Rx. Finally, the capability of controlling LoC formation was also tested as denoted by case 4 in Fig. 8 (a). To further enhance the communication security through the independently steerable SBA antennas, one of the three SBA main beams was intentionally switched to different angles. The main beam of the SBA3 was initially set to -6° toward the target Rx for the desired LoC of the target Rx. Then,

the main beam was varied up to 18° . The measured EVM decreased to 14.23 % at $\Delta\phi = 6^\circ$ and further rose more than 25 % at $\Delta\phi = 18^\circ$ as displayed in Fig. 8 (e). Thus, the proposed multibeam-based SBA was validated for high-efficiency QPSK combination to create high-order QAM signals and improve communication security through LoC formation and control. Although bit error rate (BER) measurement is essential for verifying communication performance, the use of USRP could not guarantee accurate measurements. Instead, this paper focuses on PAE and EVM performances through synthesizing multiple QPSK beams, indicating the feasibility of SBA architecture in terms of hardware functionality.

4. Conclusion

In this work, a new high-efficiency and secured communication system with a multibeam-based SBA architecture was proposed and verified at 28 GHz. Multiple SBA units were able to individually transmit QPSK signals to form high-order QAM signals with independently steerable main beams. Using the multiple QPSK signals instead of high-order QAM signals alone, drastic efficiency degradation at PA back-off operation could be solved. For the tested PA of the BFIC, 36.1 % PAE was dropped for 6-dB back-off from the P1-dB PAE, implying the high-efficiency operation of the proposed architecture. Furthermore, the proposed system was fully verified with the reference target Rx and eavesdropper Rx at 28 GHz. Three QPSK sets were transmitted through the fabricated SBA units, and the 64-QAM constellation was retrieved with the measured EVM of 4.72 %. Furthermore, the measured EVM of the eavesdropper Rx at different distances from the target Rx was more than 25 % as the spacing increased to 0.3 m. Because the conventional transmission of 64-QAM showed an EVM less than 8.5 % at the same position, higher communication security could be achieved. Lastly, the LoC control was tested by intentionally switching one of the three SBA main beams. Because of the collapse of LoC, 64-QAM signals could not be retrieved at the Rx, making the SBA steering sequence a potential data stream code to further enhance the communication security. Thus, both high efficiency and improved security performances were verified, and the proposed architecture could be a good candidate for next-generation mmWave phased array applications.

Declaration of competing interest

The authors declare that they have no known competing financial interests or personal relationships that could have appeared to influence the work reported in this paper.

Acknowledgments

This research was supported in part by the Development of Civil Military Technology Project from the Institute of Civil Military

Technology Cooperation (ICMTC) under Grant 21-CM-RA-02, and in part by the Korea Institute for Advancement of Technology (KIAT) grant funded by the Korea Government (MOTIE) (P0017011, HRD Program for Industrial Innovation).

References

- [1] S.A. Busari, K.M.S. Huq, S. Mumtaz, L. Dai, J. Rodriguez, Millimeter-wave massive MIMO communication for future Wireless systems: a survey, *IEEE Commun. Surv. Tutorials* 20 (2) (Secondquarter 2018.) 836–869.
- [2] P. Zhang, J. Chen, X. Yang, N. Ma, Z. Zhang, Recent research on massive MIMO propagation channels: a survey, *IEEE Commun. Mag.* 56 (12) (2018) 22–29.
- [3] S. Han C. -I, I. Z. Xu and C. Rowell, Large-scale antenna systems with hybrid analog and digital beamforming for millimeter wave 5G *IEEE Commun. Magazine*, 53 1 2015 186 194.
- [4] P.K. Singya, P. Shaik, N. Kumar, V. Bhatia, M.-S. Alouini, A survey on higher-order QAM constellations: technical challenges, recent advances, and future trends, *IEEE Open J. Commun. Soc.* 2 (2021) 617–655.
- [5] S.-A. Li, et al., Enabling Technology in High-Baud-Rate Coherent Optical Communication Systems, *IEEE Access* 8 (2020) 111318–111329.
- [6] A.F. Molisch, et al., Hybrid beamforming for massive MIMO: a survey, *IEEE Commun. Mag.* 55 (9) (2017) 134–141.
- [7] R. Chataut, R. Akl, "Massive MIMO systems for 5G and beyond networks-overview, recent trends, challenges, and future Research direction, *Sensors* 20 (10) (2020) 2753.
- [8] I. Ahmed, et al., A survey on hybrid beamforming techniques in 5G: architecture and system model perspectives, *IEEE Commun. Surv. Tutorials* 20 (4) (Fourthquarter 2018.) 3060–3097.
- [9] E. Ng, Y. Beltagy, G. Scarlato, A. Ben Ayed, P. Mitran, S. Boumaiza, Digital predistortion of millimeter-wave RF beamforming arrays using low number of steering angle-dependent coefficient sets, *IEEE Trans. Microwave Theory Techniques* 67 (11) (2019) 4479–4492.
- [10] M.M. Mowla, et al., Comparative performance analysis of different modulation techniques for PAPR reduction of OFDM signal, *Int. J. Comput. Networks Commun. (IJCNC)* 6 (3) (2014) 63–73.
- [11] F. Jalili, F.F. Tafuri, O.K. Jensen, Y. Li, M. Shen, G.F. Pedersen, Linearization trade-offs in a 5G mmWave active phased Array OTA setup, *IEEE Access* 8 (2020) 110669–110677.
- [12] S. Rajagopal, S. Abu-Surra and J. Zhang, "Spectral mask filling for PAPR reduction in large bandwidth mmWave systems," 2015 IEEE 16th International Workshop on Signal Processing Advances in Wireless Communications (SPAWC), Stockholm, Sweden, pp. 131-135, 2015.
- [13] W. Hong, et al., Multibeam antenna technologies for 5G Wireless communications, *IEEE Trans. Antennas Propag.* 65 (12) (2017) 6231–6249.
- [14] X. Gao, L. Dai, A.M. Sayeed, Low RF-complexity technologies to enable millimeter-wave MIMO with Large antenna Array for 5G Wireless communications, *IEEE Commun. Mag.* 56 (4) (2018) 211–217.
- [15] E.G. Larsson, O. Edfors, F. Tufvesson, T.L. Marzetta, Massive MIMO for next generation wireless systems, *IEEE Commun. Mag.* 52 (2) (2014) 186–195.
- [16] A.L. Swindlehurst, E. Ayanoglu, P. Heydari, F. Capolino, Millimeter-wave massive MIMO: the next wireless revolution? *IEEE Commun. Mag.* 52 (9) (2014) 56–62.
- [17] K. Kouassi, G. Andrieux, J.F. Diouris, PAPR distribution for single carrier M-QAM modulations, *Wireless Pers Commun.* 104 (2019) 727–738.
- [18] S. Mazahir, S.A. Sheikh, On companding schemes for PAPR reduction in OFDM systems employing higher order QAM, *IEEE Trans. Broadcast.* 62 (3) (2016) 716–726.
- [19] T. Arbi, Z. Ye, B. Geller, Low-complexity blind PAPR reduction for OFDM systems with rotated constellations, *IEEE Trans. Broadcast.* 67 (2) (2021) 491–499.
- [20] J. Kim, H.L. Lee, High gain Planar segmented antenna for mmWave phased Array applications, *IEEE Trans. Antennas Propag.* 70 (7) (2022) 5918–5922.